Atmos. Meas. Tech., 7, 1385–1394, 2014
www.atmos-meas-tech.net/7/1385/2014/
doi:10.5194/amt-7-1385-2014

Atmospheric Measurement Techniques
Open Access

DIAL measurement of lower tropospheric ozone over Saga (33.24° N, 130.29° E), Japan, and comparison with a chemistry–climate model

O. Uchino[1,2], T. Sakai[2], T. Nagai[2], I. Morino[1], T. Maki[2], M. Deushi[2], K. Shibata[2], M. Kajino[2], T. Kawasaki[3], T. Akaho[3], S. Takubo[3], H. Okumura[3], K. Arai[3], M. Nakazato[4], T. Matsunaga[1], T. Yokota[1], S. Kawakami[5], K. Kita[6], and Y. Sasano[1]

[1]National Institute for Environmental Studies, 16-2 Onogawa, Tsukuba, Ibaraki 305-8506, Japan
[2]Meteorological Research Institute, 1-1 Nagamine, Tsukuba, Ibaraki 305-0052, Japan
[3]Saga University, 1 Honjou, Saga, Saga 840-8502, Japan
[4]Japan Meteorological Agency, 1-3-4 Otemachi, Chiyoda-ku, Tokyo 100-8122, Japan
[5]Japan Aerospace Exploration Agency, 2-1-1 Sengen, Tsukuba, Ibaraki 305-8505, Japan
[6]Ibaraki University, 2-1-1 Bunkyo, Mito, Ibaraki 310-8512, Japan

Correspondence to: O. Uchino (uchino.osamu@nies.go.jp)

Received: 2 October 2013 – Published in Atmos. Meas. Tech. Discuss.: 14 January 2014
Revised: 1 April 2014 – Accepted: 1 April 2014 – Published: 21 May 2014

Abstract. We have improved an ozone DIfferential Absorption Lidar (DIAL) system, originally developed in March 2010. The improved DIAL system consists of a Nd:YAG laser and a 2 m Raman cell filled with 8.1×10^5 Pa of CO_2 gas which generate four Stokes lines (276, 287, 299, and 312 nm) of stimulated Raman scattering, and two receiving telescopes with diameters of 49 and 10 cm. Using this system, 44 ozone profiles were observed in the 1–6 km altitude range over Saga (33.24° N, 130.29° E) in 2012. High-ozone layers were observed at around 2 km altitude during April and May. Ozone column amounts within the 1–6 km altitude range were almost constant (19.1 DU on average) from January to March, and increased to 26.7 DU from late April to July. From mid-July through August, ozone column amounts decreased greatly to 14.3 DU because of exchanges of continental and maritime air masses. Then in mid-September they increased again to 22.1 DU within 1−6 km, and subsequently decreased slowly to 17.3 DU, becoming almost constant by December.

The Meteorological Research Institute's chemistry–climate model version 2 (MRI-CCM2) successfully predicted most of these ozone variations with the following exceptions. MRI-CCM2 could not predict the high-ozone volume mixing ratios measured at around 2 km altitude on 5 May and 11 May, possibly in part because emissions were assumed in the model to be constant (climatological data were used). Ozone volume mixing ratios predicted by MRI-CCM2 were low in the 2–6 km range on 7 July and high in the 1–4 km range on 19 July compared with those measured by DIAL.

1 Introduction

Ozone is an important air pollutant that at high concentrations impacts on human health and ecosystems including crops (Parrish et al., 2012). Tropospheric ozone has two main sources: photochemical production in the troposphere and downward transport from the stratosphere. Tropospheric ozone is mainly produced from nitrogen oxides (NO_x), carbon monoxide (CO), and volatile organic compounds (VOCs) by photochemical reactions. More specifically in Asia, emissions of these ozone precursors increased between 1980 and 2003 (Ohara et al., 2007). In China in particular, NO_x increased from 1996 through 2004 (Zhang et al., 2007). Summertime ozone concentrations in the 0–3 km altitude range over Beijing increased at the rate of 3 % yr^{-1} from 2002 to 2010 (Wang et al., 2012). Ozone is also a greenhouse

gas that plays an important role in climate change. The radiative forcing due to tropospheric ozone is the third strongest after carbon dioxide and methane (IPCC, 2007).

In recent years, high concentrations of surface ozone have been observed from April through June in the Kyushu district of western Japan (http://www.env.go.jp/air/osen/). In 2011, we deployed an ozone DIfferential Absorption Lidar (ozone DIAL) system, originally developed by the National Institute for Environmental Studies (NIES) at Tsukuba, at Saga (33.24° N, 130.29° E) in the Kyushu district, with three aims: (1) to validate GOSAT (Greenhouse gases Observing SATellite) ozone products retrieved from thermal infrared spectral radiances by the Thermal And Near infrared Sensor for carbon Observation-Fourier Transform Spectrometer (TANSO-FTS) onboard GOSAT (Ohyama et al., 2012); (2) to detect high-ozone concentrations in the lower troposphere; and (3) to compare the observed concentrations with concentration data predicted by the Meteorological Research Institute's (MRI) chemistry–climate model, version 2 (MRI-CCM2) (Deushi and Shibata, 2011). Except in summer, Saga is downwind of the Asian continent most of the year. Thus, if DIAL can be used to detect high-ozone concentrations, then inputting DIAL data into MRI-CCM2 will allow us to make useful predictions for photochemical oxidant advisories. In Sect. 2, we describe the ozone DIAL system, including some improvements made since 2011 and comparisons with ozonesonde data, and we describe MRI-CCM2 in Sect. 3. In Sect. 4, we present observational results obtained by the ozone DIAL system and compare them with MRI-CCM2 predictions. Section 5 is a summary and our conclusions.

2 Ozone DIAL system, data analysis and comparison with ozonesonde results

Tropospheric ozone DIAL systems have been first developed using tunable dye lasers (Gibson and Thomas, 1975; Pelon and Mégie, 1982; Browell et al., 1983; Proffitt and Langford, 1997; Kuang et al., 2013). Later Stokes lines from stimulated Raman scattering (SRS) of pressurized gas pumped by excimer lasers (Uchino et al., 1983; Kempfer et al., 1994; Eisele et al., 1999) and by Nd:YAG lasers (Ancellet et al., 1989; Sunesson et al., 1994; McDermid et al., 2002; Papayannis et al., 2005; Nakazato et al., 2007; Apituley et al., 2010) were used. In 2010, we developed a tropospheric ozone DIAL system at NIES (Uchino et al., 2011) that was installed in a container with dimensions of about 228 cm × 683 cm × 255 cm. The system's transmitter transmits laser beams at three Stokes lines (276.2 nm, 287.2 nm, and 299.1 nm) of the SRS of carbon dioxide (CO_2) with vibrational shift of 1385 cm^{-1} pumped by the fourth harmonic (266 nm) of a Nd:YAG laser (Nakazato et al., 2007; Seabrook et al., 2011).

We used this transmitter with a coaxial receiving system with a 49 cm diameter Newtonian reflecting telescope to measure ozone profiles from a few hundred meters to about 10 km altitude. However, the signal-induced bias (SIB) from the photomultiplier tubes (PMTs) limited the measurement altitude to below about 6 km (Sunesson et al., 1994; Proffitt and Langford, 1997). A mechanical chopper with a fast rising time could suppress the SIB (Uchino and Tabata, 1991; McDermid et al., 2002; Godin-Beekmann et al., 2003; Apituley et al., 2010), but there was not enough space in the container to add a mechanical chopper to the DIAL receiving system. Therefore, in January 2012 we modified the coaxial receiving system by adding a mirror in biaxial configuration. In the biaxial system, the Stokes lines were transmitted upward by a 10 cm diameter mirror with 90 % reflectivity that was set at a distance of 25 cm from the edge of the 49 cm telescope, while about 10 % of the laser energy was used to measure low-altitude ozone by the original coaxial system. Thus by adding the biaxial system, we could measure ozone profiles up to about 10 km; however, it was time-consuming to measure ozone profiles from 1 to 10 km by alternating between biaxial and coaxial measurements.

To be able to measure tropospheric ozone profiles simultaneously in the altitude range of 0.3–10 km, we introduced an additional new 10 cm diameter Newtonian receiving telescope in September 2012, using a 1.8 mm diameter quartz optical fiber to transmit the receiving light from the position of the iris of the 10 cm telescope to the entrance of a spectrometer. A dichroic beamsplitter with a 15° incidence angle efficiently separated the signal into two wavelengths, 276 and 287 nm. Furthermore, we tested the use of a fourth Stokes line (312.0 nm) of SRS from CO_2 for ozone measurement up to 15−20 km on a clear night by two wavelengths of 299 and 312 nm.

A block diagram of the improved DIAL system is shown in Fig. 1. The maximum output pulse energy of the Nd:YAG laser (Quantel YG981C) is 107 mJ per pulse at 266 nm; however the normal averages of the output energies are 70–85 mJ at 266 nm. The laser beam is collimated into the center of a 2 m long Raman cell, which consists of a stainless-steel tube with a diameter of 35 mm and 10 mm thick UV-grade quartz windows with an anti-reflective (AR) coating. The input window is a lens with a focal length $f_1 = 1100$ mm. The output energy at 312.0 nm is not measured, but CO_2 pressure is set to be 8.1×10^5 Pa because the largest receiving signal is obtained at 312.0 nm. At 8.1×10^5 Pa of CO_2 pressure and a pumping energy of 107 mJ at 266 nm, the output energies of the three Stokes lines at S1: 276.2, S2: 287.2, and S3: 299.1 nm are 7.5, 9.1, and 8.4 mJ, respectively. A pumping energy of more than 90 mJ at 266 nm is necessary for DIAL measurement using the Stokes lines at 299 nm and 312 nm.

The four Stokes lines are expanded by a factor of about 3.9 by a 50 mm diameter quartz lens with a focal length $f_2 = 4290$ mm. The beam divergence of the four Stokes lines transmitted into the atmosphere is about 0.1 mrad. The full

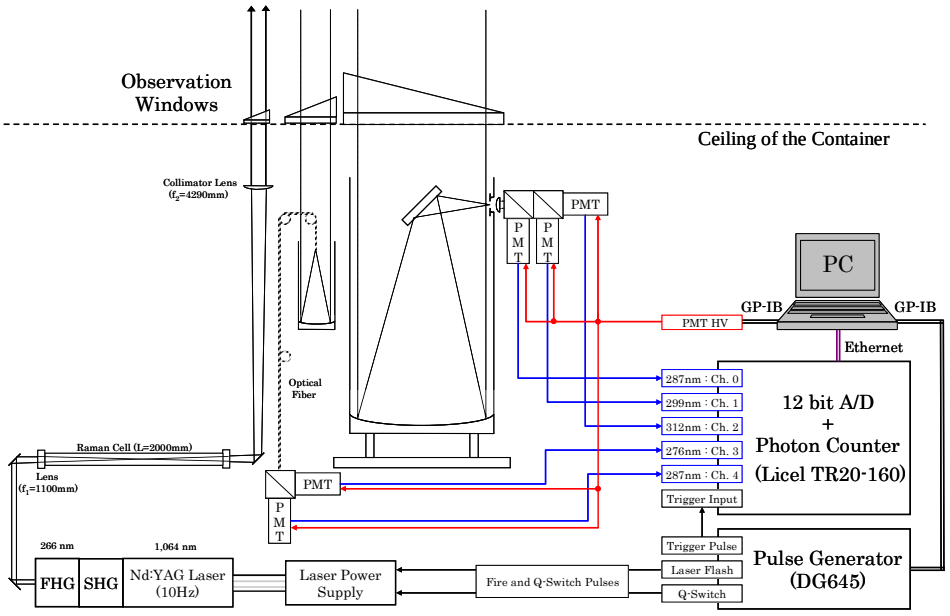

Figure 1. Block diagram of tropospheric ozone DIAL system.

field of views of the 49 cm and 10 cm telescope are 1.0 and 3.0 mrad, respectively. The system uses PMTs (Hamamatsu R3235-01) to detect the backscattered light from the atmosphere. For signal processing, a 12 bit A/D converter and photon counter (Licel TR20-160) are used. The timing of the DIAL system is controlled by a delay/pulse generator (Stanford Research Systems DG645). The specifications of this ozone DIAL system are summarized in Table 1.

The ozone number density is derived from the DIAL signals at the two wavelengths (Uchino and Tabata, 1991). The raw data were obtained with 7.5 m range resolution and 1 min integration time (i.e., 600 shots). The analog and photon counting signals for each receiving wavelength channel in Fig. 1 were connected to get high-dynamic range. To increase the signal-to-noise ratio, the integrated spatial range interval (Δz) was varied from 75 to 375 m with increasing altitude. Ozone number concentration profiles were computed from the differential of the logarithm of the ratio of the signals by fitting a third-order polynomial to nine adjacent signals by the least-mean-squares method (Fujimoto and Uchino, 1994). The effective vertical resolution was about $9 \cdot \Delta z \cdot 0.4 = 3.6 \cdot \Delta z$, which was estimated from the full-width half-maximum ozone profiles retrieved when an impulse function of ozone density was input (Beyerle and McDermid, 1999). To calculate atmospheric molecular extinction, we used the atmospheric molecular extinction cross section (Bucholtz, 1995) and the atmospheric molecular density obtained from radiosonde data at the Fukuoka District Meteorological Observatory (33.58° N, 130.38° E). The ozone absorption cross sections were calculated by taking temperature dependence into account (Bass, 1984). The ozone volume mixing ratio

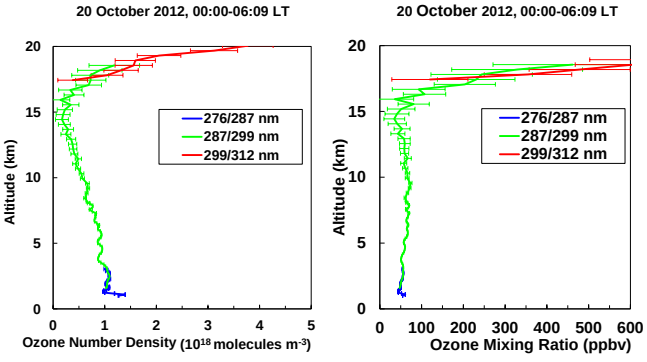

Figure 2. Vertical profiles of ozone number density (left panel) and ozone volume mixing ratio (right panel) over Saga observed by DIAL on 20 October 2012. The error bars show the statistical errors calculated from the lidar signal to noise ratios.

was also calculated from the molecular density, including water vapor.

An example of DIAL measurements using four wavelengths, including 312 nm, is shown in Fig. 2. In this case, vertical profiles of the ozone number density and volume mixing ratio are plotted together with their statistical errors (precision) calculated from the lidar signal-to-noise ratios (Uchino and Tabata, 1991). A different wavelength pair was used for each of three altitude ranges to adapt to different ozone optical depths: 276/288 nm for 1.0–3.0 km ($\Delta z = 75$ m), 287/299 nm for 1.6–8.0 km ($\Delta z = 150$ m) and 8.0−18.6 km ($\Delta z = 375$ m), and 299/312 nm for 17.4–20.8 km ($\Delta z = 375$ m). The integration time was about 6 h to observe ozone vertical profiles up to 20 km (Fig. 2), but

Table 1. Characteristics of tropospheric ozone DIAL system.

Transmitter					
Pump laser	Nd:YAG				
Wavelength	266 nm				
Pulse energy	107 mJ				
Pulse repetition rate	10 Hz				
Pulse width	8 ns				
Raman active gas	CO_2				
Stokes lines	276 nm	287 nm	299 nm	312 nm	
Pulse energy	7.5 mJ	9.1 mJ	8.4 mJ	No. meas.	
Beam divergence	0.1 mrad				
Receiver					
Telescope type	Newtonian			Prime focus (fiber coupled)	
Telescope diameter	49 cm			10 cm	
Focal length	1750 mm			320 mm	
Field of view	1 mrad			3 mrad	
Wavelength	287 nm	299 nm	312 nm	276 nm	287 nm
Bandwidth	1.02 nm	1.15 nm	0.82 nm	1.07 nm	1.05 nm
Transmission	0.18	0.32	0.36	0.17	0.21
Detector	PMT (Hamamatsu R3235-01)				
Signal processing	12 bit A/D + Photon counting				
Time resolution	1 min				
Altitude resolution	7.5 m				

ozone vertical profiles up to 6 km were usually obtained within 30 min. From January to September 2012, we generally used an integration time of about 1–3 h for biaxial and coaxial DIAL measurements, thus the resulting measurement errors were larger than those shown in Fig. 2. In this paper, we present the 2012 ozone data for altitudes lower than 6 km, measured by the DIAL system using three wavelengths (276, 287, and 299 nm). In this DIAL data analysis, the systematic uncertainty (accuracy) due to particulate backscatter and extinction was not taken into account. However, systematic uncertainty is probably on the order of 10–15 % in the planetary boundary layer and smaller than that in the free troposphere (Nakazato et al., 2007), although it can reach high values due to the presence of high-aerosol loadings and the large-aerosol concentration gradient at the top of the planetary boundary layer (Papayannis et al., 1990).

We compared our DIAL measurement with ozonesonde data (Thompson et al., 2011) (Fig. 3). The ozonesondes used were composed of an ECC ozone sensor (ENSCI-Z) and a GPS radiosonde (Meisei RS-06G). The precision and accuracy of the ozone sensor were ±4 % and ±5 % at 1000 hPa and ±12 % and ±12 % at 200 hPa, respectively, and the vertical resolution of the sensor was 300 m (http://www.dropletmeasurement.com/products/airborne/ECC_Ozonesonde). Two ozonesondes were launched by the Japan Weather Association under contract with NIES, and the measurements used in our comparison were made on 9 and 15 January 2013. The ozonesonde and DIAL measurement times were from 12:31 to 13:53 LT and from 12:46 to 13:30 LT, respectively, on 9 January. On 15 January, the ozonesonde measurement time was from 12:31 to 14:04 LT under cloudy conditions, and we used DIAL data obtained from 14:00 to 17:04 LT under comparatively clear weather conditions for the comparison.

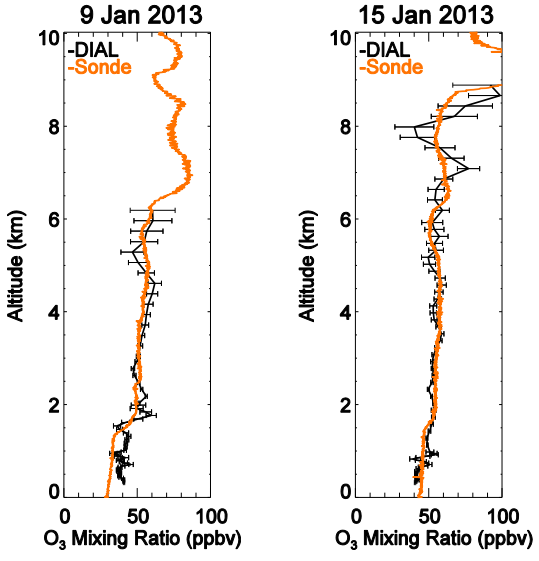

Figure 3. Comparison of ozone DIAL (black) and ECC ozonesonde (orange) measurements on 9 (left panel) and 15 January (right panel) in 2013. The error bars of ozone DIAL data show the statistical errors calculated from the lidar signal to noise ratios.

The vertical resolution of the DIAL measurement was 110 m in the lower altitude range and 830 m in the upper altitude range. Within their measurement errors, the ozonesonde and DIAL data were consistent below an altitude of 6 km (Fig. 3). The average and one standard deviation of the difference between DIAL and ozonesonde data are 14 ± 10 % below 2 km, 6 ± 4 % for 2–7 km, and 20 ± 13 % above 7 km.

3 MRI-CCM2

The MRI-CCM2 model uses chemical and physical processes from the surface to the stratosphere to simulate the global distribution and evolution of ozone and other trace gases (Deushi and Shibata, 2011). The previous version (MRI-CCM1) was a stratospheric chemistry–climate model (Shibata et al., 2005). Version 2, however, incorporates an elaborated mechanism for HO_x–NO_x–CH_4–CO photochemistry and mechanisms for the degradation of non-methane hydrocarbons and heterogeneous tropospheric reactions of aerosols, so it can simulate tropospheric ozone chemistry as well as stratospheric chemistry. Deushi and Shibata (2011) showed that MRI-CCM2 can reproduce reasonably well the observed seasonal variations of the monthly means of ozone and carbon monoxide in the troposphere. This model is currently used to predict the distribution of photochemical oxidants near the surface in support of operational air-quality forecasts of the Japan Meteorological Agency (JMA). As first step toward better air quality prediction using the model, it is necessary to evaluate MRI-CCM2 by various observational data. It is important to compare ozone data predicted by the model with not only surface ozone data but also vertical ozone data.

The chemistry module of MRI-CCM2 considers 90 chemical species, 231 homogeneous gas-phase chemical reactions (172 chemical kinetic reactions and 59 photolysis reactions), and 16 heterogeneous reactions, and it incorporates grid-scale transport with a semi-Lagrangian scheme, sub-grid-scale convective transport and turbulent diffusion, dry and wet deposition, and emissions of trace gases from various sources. The chemistry module is coupled with an MRI atmospheric general circulation model (MRI-AGCM3; Yukimoto et al., 2011) via a simple coupler (Yoshimura and Yukimoto, 2008). The chemistry module receives meteorological and radiation fields and surface conditions from MRI-AGCM3. The horizontal coordinate system of MRI-CCM2 is a Gaussian grid with a resolution of about 110 km. In the vertical, a hybrid p–σ coordinate system is used, with 48 layers from the surface to the top of the atmosphere (0.01 hPa $\approx$ 80 km). In the hybrid p–σ coordinate system, the vertical coordinate is a terrain-following σ coordinate ($\sigma = p/p_s$) near the surface, and it gradually changes to a pressure coordinate (p coordinate) near the top. The vertical resolution increases from about 100 to 600 m from the surface to 6 km. The time step of the transport (chemistry) scheme is 30 (15) min.

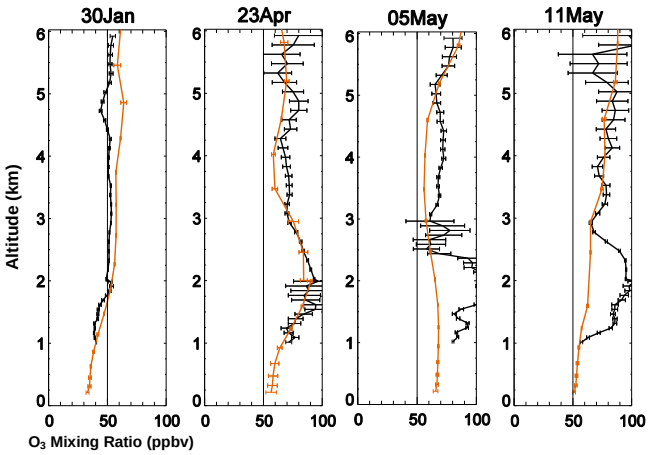

Figure 4. Vertical profiles of ozone volume mixing ratios over Saga measured by DIAL (black lines) and predicted by MRI-CCM2 (orange lines) on 30 January, 23 April, 5 and 11 May in 2012. The error bars shows the statistical errors calculated from the signal to noise ratios for the lidar and the standard deviation for the period predicted by MRI-CCM2.

In this study, the horizontal wind field in AGCM3 was forced toward the observed field by using a nudging assimilation with an 18 h e-folding time. JMA operational analysis data were used as the observed wind field for the nudging assimilation. In the chemistry module, trace-gas emissions from the burning of fossil fuels by industrial activities and aircraft (anthropogenic sources), from biomass burning (anthropogenic and natural sources), and from vegetation, soils, and the ocean (natural sources) were prescribed. Global anthropogenic emission data, except those from East Asia, were obtained from the inventory in the Emission Database for Global Atmospheric Research (EDGAR) v2.0 (Olivier et al., 1996) modified by the seasonal adjustments of Müller (1992). For East Asia, the prescribed data were obtained from an inventory of Asian anthropogenic emissions, the Regional Emission inventory in ASia (REAS), version 1.1 (Ohara et al., 2007). Biogenic and oceanic emissions were taken from Horowitz et al. (2003) and references therein. Emission of NO_x from lightning was diagnosed at 6 h intervals in the chemistry module by using the meteorological fields from AGCM3 (for details, see Deushi and Shibata, 2011). Emission of trace gases from biomass burning, which depends on the height above ground, is based on the Description of EDGAR 32FT2000(v8) (http://www.rivm.nl/edgar/Images/Description_of_EDGAR_32FT2000(v8)_tcm32-22222.pdf). Present-day concentrations of N_2O, CH_4, chlorofluorocarbons, and halons were prescribed at the surface. In this paper we used the data output by the model every hour for the comparison with the DIAL-observed data in this study.

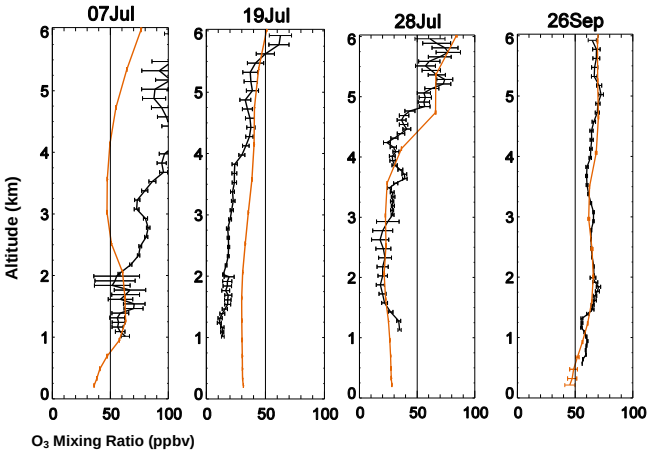

Figure 5. Same as Fig. 4 but for 7, 19, and 28 July, and 26 September in 2012.

4 DIAL observational results and comparison with MRI-CCM2 output

Hourly grid-point ozone data predicted by MRI-CCM2 were spatially interpolated for the Saga area, averaged over the DIAL measurement time (about 1–7 h), and then compared to our DIAL ozone data.

4.1 Vertical profiles

At first the vertical profiles of lower tropospheric ozone in the altitude range of 1–6 km measured by DIAL between January and May 2012 are compared with MRI-CCM2 predictions (Fig. 4). The DIAL-measured ozone volume mixing ratios on 30 January, about 40–50 ppbv, were successfully predicted by MRI-CCM2, except in the 4–5 km altitude range. High-ozone values were measured at around 2 km altitude in the daytime on 23 April, 5 May, and 11 May. A backward trajectory analysis suggested that the air masses linked with these high-ozone volume mixing ratios at 2 km were transported to Saga across the Yellow Sea (23 April and 5 May) or over the Korean Peninsula (11 May) from polluted areas in East China (Parrish and Zhu, 2009) within a few days. MRI-CCM2 predicted well these high-ozone densities on 23 April, but not those on 5 May or 11 May. This is possibly in part because emissions were assumed in the model to be constant (climatological data were used).

Figure 5 shows ozone profiles in the 1−6 km altitude range for July and September 2012. MRI-CCM2 was unable to predict the high-ozone values of more than 70 ppbv above 2.3 km that were measured by DIAL on 7 July. On 19 July, the measured ozone volume mixing ratios were 10–30 ppbv below about 4 km, whereas MRI-CCM2 predicted ratios of 30–40 ppbv below 4 km. On 28 July, however, MRI-CCM2 predicted well the ozone volume mixing ratios measured by DIAL of about 30–40 ppbv below 4 km. On 26 September, MRI-CCM2 predicted very well the ozone volume mixing ratios measured by DIAL of about 35–70 ppbv from 500 m to 6 km. According to the backward trajectory analysis, the air masses below 4 km with low-ozone volume mixing ratios of about 20–40 ppbv on 19 and 28 July came from the Pacific Ocean south of Saga. The ozone volume mixing ratios predicted by MRI-CCM2 for 2–6 km on 7 July were lower, and those for 1–4 km on 19 July were higher, compared with the DIAL measurements.

Figure 6 shows horizontal maps of ozone volume mixing ratio and horizontal wind predicted by MRI-CCM2 for 500 hPa (about 5.5 km altitude), 700 hPa (3 km), 800 hPa (2 km), and 850 hPa (1.5 km) pressure levels at 06:00 UTC on 7 July 2012. According to the weather chart on the same day provided by JMA (http://www.data.jma.go.jp/fcd/yoho/hibiten/index.html), the Meiyu-Baiu front extended from west to east through the center of a low-pressure system over Japan. In this prediction, the synoptic-scale pattern of horizontal-wind field is reproduced reasonably. A large north–south gradient of ozone volume mixing ratios is located near the stationary front in the lower free-troposphere. The ozone concentration is low over the southern part of the front because of the chemical destruction in the summertime marine air mass, whereas high-ozone level area is present over the northern part of the front. During the DIAL observing period the large gradient of ozone concentration was located near the Saga site in the lower free-troposphere (Fig. 6). This suggests that one of the possible reasons for the significant discrepancy between the DIAL ozone profile and the predicted one (Fig. 5) is that the meso-scale front structure and its position are not fully captured by the model due to its coarse spatial resolution. In addition, it is plausible that model transport with the coarse grid does not reproduce well fine-scale structures of air (trace gases) filaments.

4.2 Lower tropospheric ozone column

Figure 7 shows time variations of the lower tropospheric ozone column amounts within the 1–6 km and 1–2 km altitude ranges over Saga in 2012 as measured by DIAL and predicted by MRI-CCM2. Because of restricting weather conditions, DIAL measurements were obtained only twice in May and twice in June, but at least three measurements were obtained in each of the other months. In 2012, the ozone column amounts showed an approximately seasonal variation except for a dip from early July through mid-September. Column amounts within 1–6 km were almost constant from January to early March, and then increased until late June. The maximum value in the 1–6 km range was 7.82×10^{21} molecules m^{-2}, corresponding to 29.1 DU ($1\,DU = 2.688 \times 10^{20}$ molecules m^{-2}), on 22 June 2012. Thereafter, ozone column amounts within the 1−6 km range decreased in early August, but with large variations. The minimum value within the 1–6 km range of 2.28×10^{21} molecules m^{-2} (8.5 DU) was observed on

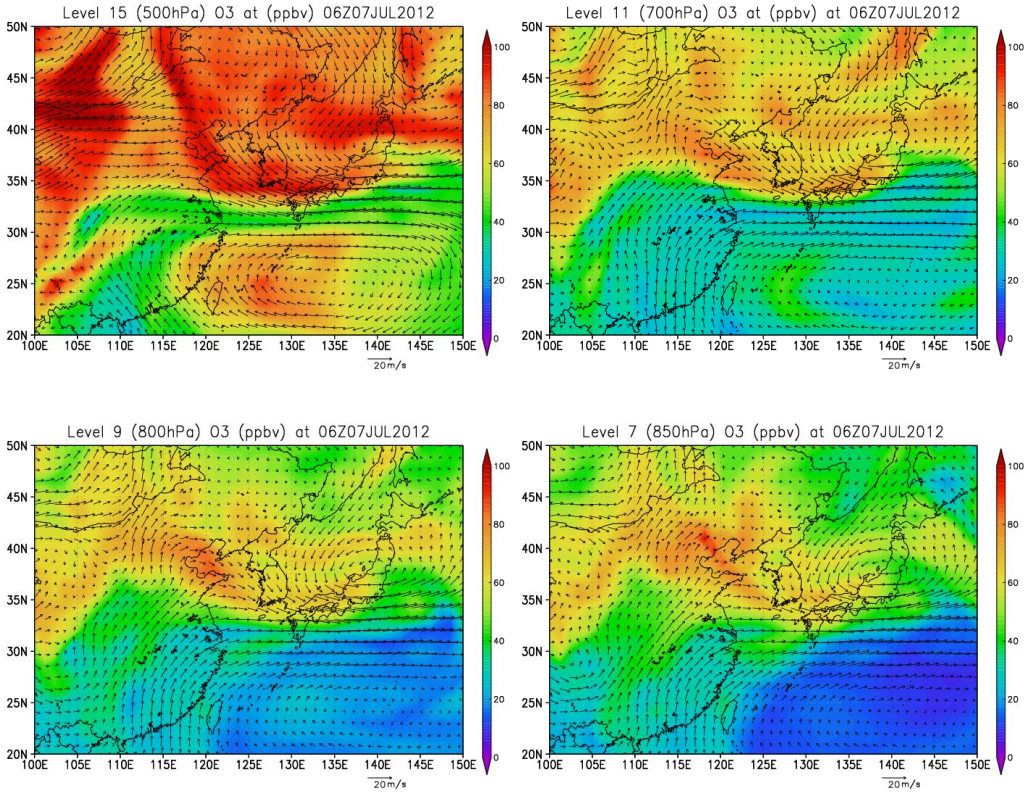

Figure 6. Horizontal maps of ozone volume mixing ratio in ppbv and horizontal wind in m s^{-1} predicted by MRI-CCM2 for 500, 700, 800, 850 hPa pressure levels at 06:00 UTC on 7 July 2012.

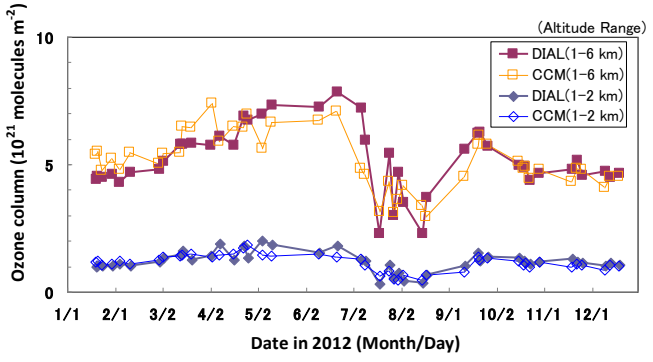

Figure 7. Ozone columns for 1–6 km and 1–2 km altitude ranges over Saga in 2012 measured by DIAL and predicted by MRI-CCM2.

15 August 2012. These variations are due to possibly exchange events between the ozone-rich continental and the ozone-poor maritime air masses. Subsequently, ozone column amounts increased again in mid-September, and then decreased slowly, becoming almost constant by December, when the ozone column amount within the 1−6 km range was 4.65×10^{21} molecules m^{-2} (17.3 DU). The results predicted by MRI-CCM2 were mainly consistent with our DIAL observational results.

The temporal variation of the ozone column values within the 1−2 km range in 2012 was similar to that in the 1–6 km range. The mean value was about 1.03×10^{21} molecules m^{-2} (3.8 DU) from 20 January to 11 February. Then, the ozone column amount increased to a maximum value of 2.02×10^{21} molecules m^{-2} (7.5 DU) on 5 May, followed by a decreased value down to 0.32×10^{21} molecules m^{-2} (1.2 DU) on 19 July. Moreover the mean ozone column amount within the 1–2 km range was about 0.55×10^{21} molecules m^{-2} (2.0 DU) from 28 July to 18 August. Subsequently, the column ozone value increased to more than 1.0×10^{21} molecules m^{-2} (3.7 DU) by 19 December. MRI-CCM2 predicted similar variations of the ozone column amounts within the 1–2 km range, but the predicted values were lower than the DIAL measurements on 5 and 11 May and 22 June.

5 Concluding remarks

With our improved DIAL system, 44 ozone profiles were observed in the 1–6 km altitude range over Saga in 2012. High-ozone layers were observed at around 2 km altitude during April and May. Ozone column amounts within the 1–6 km altitude range were almost constant (19.1 DU) from January to March, and increased to 26.7 DU from late April to

July. From mid-July through August, ozone column amounts showed large variations (8.5–22.0 DU), attributed to exchanges between continental and maritime air masses. Ozone column amounts within the 1–6 km range increased again to mid-September, then decreased slowly to 17.3 DU and became almost constant through December.

MRI-CCM2 successfully predicted these ozone variations with the following exceptions. MRI-CCM2 could not predict the high-ozone volume mixing ratios measured at around 2 km altitude on 5 May and 11 May, possibly in part because emissions (especially from open biomass burning) were assumed in the model to be constant (climatological data were used). Ozone volume mixing ratios predicted by MRI-CCM2 were low in the 2–6 km range on 7 July and high in the 1–4 km range on 19 July compared with those measured by DIAL.

A major benefit of ozone DIAL is that it can measure continuously vertical ozone profiles with high-vertical and high-temporal resolution. The process of stratospheric ozone intrusion into the troposphere was clearly observed on 20–21 June 2001 by continuous DIAL measurement at Garmisch-Partenkichen, Germany, and the excellent data set was used for model intercomparisons and validation (Roelofs et al., 2003; Zanis et al., 2003; Stohl et al., 2003). On the other hand, the ability of a regional air quality model was evaluated to reproduce summertime ozone pollution over the Kanto region in Japan using quasi-continuous ozone DIAL measurement data (Niwano et al., 2007). We plan to study the process that air mass of high-ozone concentration in the free troposphere is mixed into the planetary boundary layer by continuous DIAL measurement. Further, we plan to utilize ozone DIAL data for validation of a new version of an MRI oxidant prediction system over an extended period of time. In the prediction system, a regional chemistry-transport model, known as MRI-PM/c (Kajino et al., 2012), with higher spatial resolution (20 km and/or 5 km) is nested in MRI-CCM2. The prediction system also adopts an up-to-date inventory and higher temporal resolution of biomass burning emissions. The regional model can reproduce meso-scale weather phenomena and advection of air mass. However, if boundary data for the regional model produced by the global model does not include adequate information on fine-scale structures in trace-gas distributions, the performance of the prediction system will be degraded. Therefore, in order to improve total performance of the prediction system, it is necessary to validate not only the regional model but also the global model with observation data such as ozone DIAL data and surface ozone monitoring data extensively, which enable us to estimate error coming from outside of the boundary.

Acknowledgements. We used radiosonde data measured by the Japan Meteorological Agency, and the Meteorological Data Explorer (METEX), developed by Jiye Zeng at the Center for Global Environmental Research (CGER) of NIES to calculate isentropic backward trajectories. The authors wish to thank the Editor, two anonymous referees, and M. J. Newchurch for helpful comments. This work was partly supported by JSPS KAKENHI grant number 23310018.

Edited by: G. Ehret

References

Ancellet, G., Papayannis, A., Pelon, J., and Mégie, G.: DIAL tropospheric ozone measurement using a Nd:YAG laser and the Raman shifting technique, J. Atmos. Ocean. Technol., 6, 832–839, 1989.

Apituley, A., Hoexum, M., Potma, C., and Wilson, K.: Tropospheric ozone DIAL for air quality and climate monitoring, and validation studies, Proceedings of the 25th International Laser Radar conference, St. Petersburg, 5–9 July 2010, 862–865, 2010.

Bass, A. M.: The ultraviolet absorption cross-section of ozone, Fin. Rep. NASA, Cont. No. S-40127B, 1984.

Beyerle, G. and McDermid, I. S.: Altitude range resolution of differential absorption lidar ozone profiles, Appl. Opt., 38, 924–927, 1999.

Browell, E. V., Carter, A. F., Shipley, S. T., Allen, R. J., Butler, C. F., Mayo, M. N., Siviter Jr., J. H., and Hall, W. M.: NASA multipurpose airborne DIAL system and measurements of ozone and aerosol profiles, Appl. Opt., 22, 522–534, 1983.

Bucholtz, A.: Rayleigh-scattering calculations for the terrestrial atmosphere, Appl. Opt., 34, 2765–2773, 1995.

Deushi, M. and Shibata, K.: Development of a Meteorological Research Institute Chemistry-Climate Model version 2 for the study of tropospheric and stratospheric chemistry, Pap. Meteorol. Geophys., 62, 1–46, doi:10.2467/mripapers.62.1, 2011.

Eisele, H., Scheel, H. E., Sladkovic, R., and Trickl, T.: High-resolution lidar measurements of stratosphere-troposphere exchange, J. Atmos. Sci., 56, 319–330, 1999.

Fujimoto, T. and Uchino, O.: Estimation of the error caused by smoothing on DIAL measurements of stratospheric ozone, J. Meteor. Soc. Jpn., 72, 605–611, 1994.

Gibson, A. J. and Thomas, L.: Ultraviolet laser sounding of the troposphere and lower stratosphere, Nature, 256, 561–563, 1975.

Godin-Beekmann, S., Porteneuve, J., and Garnier, A.: Systematic DIAL lidar monitoring of the stratospheric ozone vertical distribution at Observatoire de Haute-Provence (43.92° N, 5.71° E), J. Environ. Monitor., 5, 57–67, 2003.

Horowitz, L. W., Walters, S. M., Mauzerall, D. L., Emmons, L. K., Rasch, P. J., Granier, C., Tie, X., Lamarque, J.-F., Schultz, M. G., Tyndall, G. S., Orlando, J. J., and Brasseur, G. P.: A global simulation of tropospheric ozone and related tracers: description and evaluation of MOZART, version 2. J. Geophys. Res., 108, 4784, doi:10.1029/2002JD002853, 2003.

Intergovernmental Panel on Climate Change (IPCC), Climate change 2007: The Physical Science Basis: Contribution of Working Group I to the Fourth Assessment Report of the Intergovernmental Panel on Climate Change, edited by: Solomon, S., Qin, S., Manning, M., Chen, Z., Marquis, M., Averyt, K. B., Tignor, M., and Miller, H. L., Cambridge University Press, Cambridge, UK and New York, NY, USA, 996 pp., 2007.

Kajino, M., Deushi, M., Maki, T., Oshima, N., Inomata, Y., Sato, K., Ohizumi, T., and Ueda, H.: Modeling wet deposition and concentration of inorganics over Northeast Asia with MRI-PM/c,

Geosci. Model Dev., 5, 1363–1375, doi:10.5194/gmd-5-1363-2012, 2012.

Kempfer, U., Carnuth, W., Lotz, R., and Trickl, T.: A wide-range ultraviolet lidar system for tropospheric ozone measurements: development and application, Rev. Sci. Instrum., 65, 3145–3164, 1994.

Kuang, S., Newchurch, M. J., Burris, J., and Liu, X.: Ground-based lidar for atmospheric boundary layer ozone measurements, Appl. Opt., 52, 3557–3566, 2013.

McDermid, I. S., Beyerle, G., Haner, D. A., and Leblanc, T.: Redesign and improved performance of the tropospheric ozone lidar at the Jet Propulsion Laboratory Table Mountain Facility, Appl. Opt., 41, 7550–7555, 2002.

Müller, J.-F.: Geographical distribution and seasonal variation of surface emissions and deposition velocities of atmospheric trace gases, J. Geophys. Res., 97, 3787–3804, 1992.

Nakazato, M., Nagai, T., Sakai, T., and Hirose, Y.: Tropospheric ozone differential-absorption lidar using stimulated Raman scattering in carbon dioxide, Appl. Opt., 46, 2269–2279, 2007.

Niwano, M., Takigawa, M., Takahashi, M., Akimoto, H., Nakazato, M., Nagai, T., Sakai, T., and Mano, Y.: Evaluation of vertical ozone profiles simulated by WRF/Chem using lidar-observed data, SOLA, 3, 133–136, doi:10.2151/sola.2007-034, 2007.

Ohara, T., Akimoto, H., Kurokawa, J., Horii, N., Yamaji, K., Yan, X., and Hayasaka, T.: An Asian emission inventory of anthropogenic emission sources for the period 1980–2020, Atmos. Chem. Phys., 7, 4419–4444, doi:10.5194/acp-7-4419-2007, 2007.

Ohyama, H., Kawakami, S., Shiomi, K., and Miyagawa, K.: Retrievals of total and tropospheric ozone from GOSAT thermal infrared spectral radiances, IEEE Trans. Geosci. Remote Sens., 50, 1770–1784, doi:10.1109/TGRS.2011.2170178, 2012.

Olivier, J. G. J., Bouwman, A. F., van der Maas, C. W. M., Berdowski, J. J. M., Veldt, C., Bloos, J. P. J., Visschedijk, A. J. H., Zandveld, P. Y. J., and Haverlag, J. L.: Description of EDGAR version 2.0: a set of global emission inventories of greenhouse gases and ozone-depleting substances for all anthropogenic and most natural sources on a per country basis and on $1^\circ \times 1^\circ$ grid. RIVM Rep. 771060 002/TNO-MEP Rep. R96/119, National Institute of Public Health and Environment, Bilthoven, Netherlands, 1996.

Papayannis, A., Ancellet, G., Pelon, J., and Mégie, G.: Multiwavelength lidar for ozone measurements in the troposphere and the lower stratosphere, Appl. Opt., 29, 467–476, 1990.

Papayannis, A., Balis, D., Zanis, P., Galani, E., Wernli, H., Zerefos, C., Stohl, A., Eckhardt, S., and Amiridis, V.: Sampling of an STT event over the Eastern Mediterranean region by lidar and electrochemical sonde, Ann. Geophys., 23, 2039–2050, doi:10.5194/angeo-23-2039-2005, 2005.

Parrish, D. D. and Zhu, T.: Clean air for megacities, Science, 326, 674–675, doi:10.1126/science.1176064, 2009.

Parrish, D. D., Law, K. S., Staehelin, J., Derwent, R., Cooper, O. R., Tanimoto, H., Volz-Thomas, A., Gilge, S., Scheel, H.-E., Steinbacher, M., and Chan, E.: Long-term changes in lower tropospheric baseline ozone concentrations at northern mid-latitudes, Atmos. Chem. Phys., 12, 11485–11504, doi:10.5194/acp-12-11485-2012, 2012.

Pelon, J. and Mégie, G.: Ozone monitoring in the troposphere and lower stratosphere: evaluation and operation of a ground-based lidar station, J. Geophys. Res., 87, 4947–4955, 1982.

Proffitt, M. H. and Langford, A. O.: Ground-based differential absorption lidar system for day or night measurements of ozone throughout the free troposphere, Appl. Opt., 36, 2568–2585, 1997.

Roelofs, G. J., Kentarchos, A. S., Trickl, T., Stohl, A., Collins, W. J., Crowther, R. A., Hauglustaine, D., Klonecki, A., Law, K. S., Lawrence, M. G., von Kuhlmann, R., and van Weele, M.: Intercomparison of tropospheric ozone models: ozone transport in a complex tropopause folding event, J. Geophys. Res., 108, 8529, doi:10.1029/2003JD003462, 2003.

Seabrook, J. A., Whiteway, J., Staebler, R. M., Bottenheim, J. W., Komguem, L., Gray, L. H., Barber, D., and Asplin, M.: LIDAR measurements of Arctic boundary layer ozone depletion events over the frozen Arctic Ocean, J. Geophys. Res., 116, D00S02, doi:10.1029/2011JD016335, 2011.

Shibata, K., Deushi, M., Sekiyama, T. T., and Yoshimura, H.: Development of an MRI chemical transport model for the study of stratospheric chemistry, Pap. Meteorol. Geophys., 55, 75–119, 2005.

Stohl, A., Bonasoni, P., Cristofanelli, P., Collins, W., Feichter, J., Frank, A., Forster, C., Gerasopoulos, E., Gäggeler, H., James, P., Kentarchos, T., Kromp-Kolb, H., Krüger, B., Land, C., Meloen, J., Papayannis, A., Priller, A., Seibert, P., Sprenger, M., Roelofs, G. J., Scheel, H. E., Schnabel, C., Siegmund, P., Tobler, L., Trickl, T., Wernli, H., Wirth, V., Zanis, P., and Zerefos, C.: Stratosphere-troposphere exchange: a review, and what we have learned from STACCATO, J. Geophys. Res., 108, 8516, doi:10.1029/2002JD002490, 2003.

Sunesson, J. A., Apituley, A., and Swart, D. P. J.: Differential absorption lidar system for routine monitoring of tropospheric ozone, Appl. Opt., 33, 7045–7058, 1994.

Thompson, A. M., Oltmans, S. J., Tarasick, D. W., Von der Gathen, P., Smit, H. G. J., and Witte, J. C.: Strategic ozone sounding networks: review of design and accomplishments, Atmos. Environ. 45, 2145–2163, 2011.

Uchino, O. and Tabata, I.: Mobile lidar for simultaneous measurements of ozone, aerosols, and temperature in the stratosphere, Appl. Opt., 30, 2005–2012, 1991.

Uchino, O., Tokunaga, M., Maeda, M., and Miyazoe, Y.: Differential-absorption-lidar measurement of tropospheric ozone with excimer-Raman hybrid laser, Opt. Lett., 8, 347–349, 1983.

Uchino, O., Sakai, T., Nagai, T., Nakazato, M., Morino, I., Yokota, T., Matsunaga, T., Sugimoto, N., Arai, K., and Okumura, H.: Development of a mobile lidar for GOSAT product validation, J. Remote Sens. Soc. Jpn., 31, 435–445, 2011 (in Japanese).

Wang, Y., Konopka, P., Liu, Y., Chen, H., Müller, R., Plöger, F., Riese, M., Cai, Z., and Lü, D.: Tropospheric ozone trend over Beijing from 2002–2010: ozonesonde measurements and modeling analysis, Atmos. Chem. Phys., 12, 8389–8399, doi:10.5194/acp-12-8389-2012, 2012.

Yoshimura, H. and Yukimoto S.: Development of a Simple Coupler (Scup) for Earth System Modeling, Pap. Meteorol. Geophys., 59, 19–29, 2008.

Yukimoto, S., Yoshimura, H., Hosaka, M., Sakami, T., Tsujino, H., Hirabara, M., Tanaka, T. Y., Deushi M., Obata, A., Nakano, H., Adachi, Y., Shindo, E., Yabu, S., Ose, T., and Kitoh, A.: Me-

teorological Research Institute Earth System Model Version 1 (MRI-ESM1)–Model Description–, Tech. Rep. of MRI, 64, 83 pp., 2011.

Zhang, Q., Streets, D. G., He, K., Wang, Y., Richter, A., Burrows, J. P., Uno, I., Jang, C. J., Chen, D., Yao, Z., and Lei, Y.: NO_X emission trends for China, 1995–2004: the view from the ground and the view from space, J. Geophys. Res., 112, D22306, doi:10.1029/2007JD008684, 2007.

Zanis, P., Trickl, T., Stohl, A., Wernli, H., Cooper, O., Zerefos, C., Gaeggeler, H., Schnabel, C., Tobler, L., Kubik, P. W., Priller, A., Scheel, H. E., Kanter, H. J., Cristofanelli, P., Forster, C., James, P., Gerasopoulos, E., Delcloo, A., Papayannis, A., and Claude, H.: Forecast, observation and modelling of a deep stratospheric intrusion event over Europe, Atmos. Chem. Phys., 3, 763–777, doi:10.5194/acp-3-763-2003, 2003.